










# Spatiotemporal formation of the large vacuole regulated by the BIN2-VLG module is required for female gametophyte development in Arabidopsis

Li-Qin Hu <sup>1,2,3,†</sup> Shi-Xia Yu <sup>1,2,3,†</sup> Wan-Yue Xu <sup>4</sup> Song-Hao Zu,<sup>1</sup> Yu-Tong Jiang <sup>1</sup>, Hao-Tian Shi <sup>2,3</sup> Yan-Jie Zhang <sup>1</sup> Hong-Wei Xue <sup>2,3</sup> Ying-Xiang Wang <sup>4</sup> and Wen-Hui Lin <sup>1,2,\*</sup>

<sup>1</sup> Institute of Botany, Chinese Academy of Sciences, Beijing 100871, China; <sup>2</sup> Institute of Botany, Chinese Academy of Sciences, Beijing 100871, China; <sup>3</sup> Institute of Botany, Chinese Academy of Sciences, Beijing 100871, China; <sup>4</sup> Institute of Botany, Chinese Academy of Sciences, Beijing 100871, China

\*A... (W.H.L.)  
†...  
H.L...  
H...  
I...  
I... A... ( // m s ... m / / // /G H ... ) : W.H.L. (W.L.@ ... )

## Abstract

In Arabidopsis, the formation of the large vacuole (LV) is a key step in female gametophyte (FG) development. The AC/LEL, GAME, and H/E (LV) genes are involved in LV formation. The VLG module, including VLG1 and VLG2, is essential for LV formation. The BRASSINOSTEROID INSENSITIVE2 (BIN2) gene is a negative regulator of the VLG module. In this study, we investigated the spatiotemporal formation of the large vacuole regulated by the BIN2-VLG module. We found that BIN2 acts as a negative regulator of the VLG module. The VLG module is required for the formation of the large vacuole in the female gametophyte. The BIN2-VLG module is required for female gametophyte development in Arabidopsis.

Downloaded from https://academic.oup.com/plcell/advance-article/doi/10.1093/plcell/koad007/6989487 by National Science & Technology Library user on 16 February 2023

## Introduction

I A ... (FG) ...  
... (MNC) ...  
... (FM) ...  
... FG ...  
... ( ... ) ...  
... (G ... , 1990; M ... , 1994; ... , 1995; C ... , 1997).  
... FG ...  
... FG ...  
... FG ...  
... fi ...  
A ... A ABI GALAC A  
EI 18 (AG 18) (A ... -G ... -C I ... , 2004),  
B DDI G I HIBI ED  
BE INIDA LE (B B3.1) (L m ... , 2008),  
KI EI -1 m m ... A ... (A KI -1)  
(H ... , 2014), ... 88- ... m. k ...  
M DIFIE ... C1,7 (M 7) ( ... , 2014), HI ... E  
ACE L A FE A E 1 (HA 1) ... HA 2 (L ... , 2008), CH ... A I - E M DELI G 11 (CH 11)  
(H ... -M ... , 2005), ... M AD ...

AGAM ... -LIKE 23 (AGL23) (C. l. m ... , 2008),  
... FG ...  
... GA ...  
GA-LIKE1 ( GL1) ... FM  
(G. m ... , 2020). I ... m ... A ...  
... A G A E5 (AG 5)  
... fi ... ( ... , 2012). KA ... HE I E ABLI G ... A ...  
C ... LA MICH L1 (KE CH1). ... m l ...  
... L27 ... m ...  
... m ...  
... fi ... ( ... , 2020).

( $<5 \mu\text{m}$ ) ... FG2, ...  
 ... FG2. ...  
 ... 4 + 4 ... FG5  
 ( ... 1995; C ... 1997).  
 ... H ... 1993;  
 1995; C ... 1997).  
 ... VLG ...  
 C1 (DC1) ...  
 fi ...  
 (M B) ... C), ...  
 ... FG. ... /  
 VLG m ... FG ...  
 ... FG1, FG2, ...  
 ... FG5, ... FG ... FG7  
 (D'I ... 2017). I ...  
 UCCA8 ...  
 ( ... 2015), ...  
 ... FG, ...  
 ( ... 2021). B ... FG ...  
 (C TOKININ INDEPENDENT1, CK11) m ...  
 FG5. ...  
 ( ... 2002).  
 ... FG ...  
 ... 2-1, ... m ...  
 BIN2 (L ... 2001), ... m ...  
 FG ... E ... BI 2 ...  
 ... FG1, ... BI 2 ...  
 ... FG ...  
 ... F ... BI 2 ...  
 ... LG, ... LG,  
 ... FG. fi ...  
 BI 2- LG m ...  
 ... FG ... fi ...  
 ... FG ...

( ... 1995;  
 C ... 1997; ... 2005).  
 2-1 FG ... m ...  
 FG1. ... 2-1 FG ... m ...  
 ... FG (F ... 1, A ... B). H ... m ...  
 43.6% ( = 188) ...  
 ... (F ... 1, C ... ). I ...  
 9% ... (3%, = 135)  
 (F ... 1, D ... ). A ...  
 ... 2-1 m ... m ... BI 2  
 (L ... m, 2002).  
 ... BI 2 ... m ...  
 ... FG ... m ... FG1.  
 ... 2-1 m ...  
 ... m ... BIN2 ... 2-1 m ...  
 ( m ... BIN2\*) ...  
 ... SEEDSTICK (STK) m ... (L ...  
 ... 2001; ... 2003; K ... 2005;  
 ... H ... 2010; ... 2019).  
 ... 2-1, ... m ... #31 ... #32 ...  
 ... FG ... m ... ( ... m ...  
 F ... 1A). ... m ... 34.5%  
 ( = 84) ... 32.6% ( = 129) ... FG ... FG1 ...  
 #31 ... #32, ... (F ... 1, E,  
 F, H, I, ... ), ... 22.6% ... 46.5% ...  
 #31 ... #32, ... (F ... 1, G, J, ... ).  
 ... m ... BIN2 ...  
 ... FG ... m ... 2-1.  
 fi m = 1883 4 (3%, m ... m ... m ...  
 =

**Results**

**Increased BIN2 activity leads to abnormal formation of large vacuoles at stage FG1**

... FG, ... FG ...  
 ... m ...  
 ... fi ...  
 ... m ...  
 ... m ...

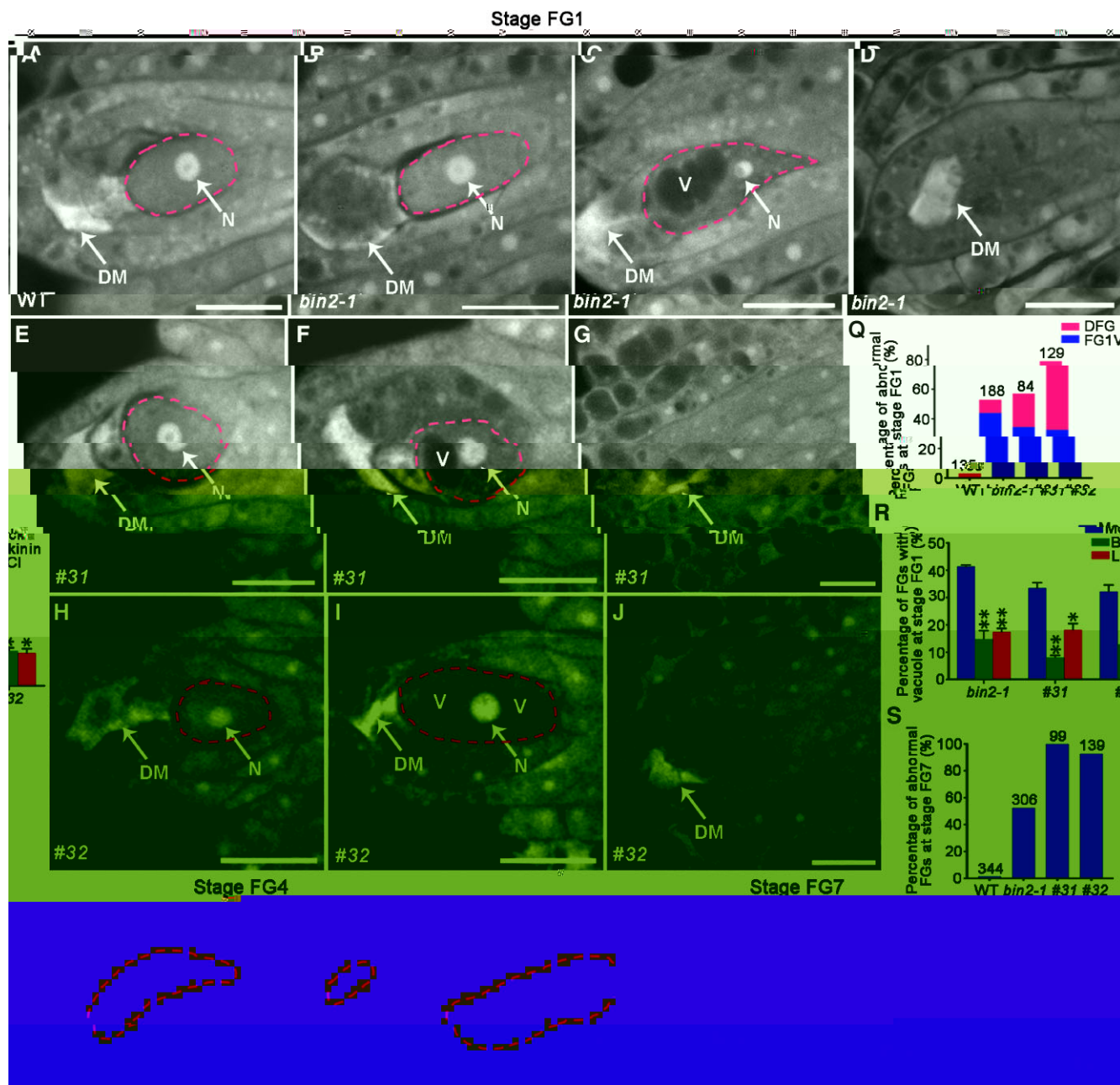


**Figure 1 |** Morphological changes and vacuolization in FG1, FG4, and FG7 stages. (A-C) WT, bin2-1, and bin2-1;#31 FG1 cells expressing GFP. (D-G) bin2-1;#31, bin2-1;#32, and bin2-1;#31;#32 FG1 cells expressing GFP. (H-I) bin2-1;#31, bin2-1;#32, and bin2-1;#31;#32 FG4 cells expressing GFP. (J-K) bin2-1;#31, bin2-1;#32, and bin2-1;#31;#32 FG7 cells expressing GFP. (L) bin2-1;#31, bin2-1;#32, and bin2-1;#31;#32 FG7 cells expressing GFP. (M-N) bin2-1;#31, bin2-1;#32, and bin2-1;#31;#32 FG4 cells expressing GFP. (O-Q) Quantification of abnormal FGs at stage FG1. (R) Quantification of abnormal FGs at stage FG1 with vacuole. (S) Quantification of abnormal FGs at stage FG7. Scale bars = 10 μm. (\*\*P < 0.01, \*P < 0.05, n.s. = not significant).

bin2-1;#31, bin2-1;#32, and bin2-1;#31;#32 FG1 cells expressing GFP. (D-G) bin2-1;#31, bin2-1;#32, and bin2-1;#31;#32 FG1 cells expressing GFP. (H-I) bin2-1;#31, bin2-1;#32, and bin2-1;#31;#32 FG4 cells expressing GFP. (J-K) bin2-1;#31, bin2-1;#32, and bin2-1;#31;#32 FG7 cells expressing GFP. (L) bin2-1;#31, bin2-1;#32, and bin2-1;#31;#32 FG7 cells expressing GFP. (M-N) bin2-1;#31, bin2-1;#32, and bin2-1;#31;#32 FG4 cells expressing GFP. (O-Q) Quantification of abnormal FGs at stage FG1. (R) Quantification of abnormal FGs at stage FG1 with vacuole. (S) Quantification of abnormal FGs at stage FG7. Scale bars = 10 μm. (\*\*P < 0.01, \*P < 0.05, n.s. = not significant).

(F 2, A & B). A FG7, 97.7%  
 FG 2.3%  
 (=348, F 2, C, D, & I). B  
 85.6% 2-3 1 2 FG  
 3.1%  
 FG1, 1.3% FG2  
 10.5% (=229, F 2, E-I).  
 BIN2  
 FG BIN2  
 FG

**BIN2 is expressed in the female gametophyte**

B BIN2  
 BIN2 FG  
 G BIN2  
 (L m, 2002). G  
 P, BIN2:GUS FG  
 FG1 FG7 (F 2A).  
 BI 2 FG, -BI 2  
 -BI 2  
 fi -BI 2  
 BI 2 (≈43, D)  
 -BI 2  
 (F 2B).  
 BI 2  
 (K m, 2009; L, 2020). F  
 BI 2  
 2-3 1 2  
 (F 2C).  
 BI 2-GF  
 P, BIN2:BIN2-GFP  
 -GF -BI 2  
 F 2C).  
 -BI 2  
 FG BI 2  
 2-3 1 2  
 2 BI 2 (F 2, D & E),  
 BI 2 FG.G  
 BIN2 FG BI 2  
 (F 2, D & E),  
 BI 2  
 B C, (C  
 m, 2016, 2020). F  
 BI 2 GF - AM 711,  
 (E m, 2011; F m, 2017) (F 2, J & K, F 3),  
 BI 2 m GF - AM 711.  
 BI 2  
 B / C FG  
 FG

**The large vacuoles are formed early in 2-1 female gametophyte development**

2-1 FG  
 M/C (P, KNU:KNU-VENUS)  
 (m, 2004; m, 2018) FM (P, FM1:GUS)  
 (H m, 2005). KNU FM1  
 2-1 FG FG0 FG1  
 (F 4A, -D),  
 2-1 FG  
 m FM1:G 2-1 FG  
 FG1, FM FG m  
 (F 4, E, -H).  
 FG1, FG  
 FG m fi H  
 P, UBQ10:  
 GFP-VAMP711 2-1 m  
 B FG1  
 FG1).  
 m FG1 (F 3, A & D),  
 m FG1  
 (F 3, B & E),  
 m  
 FG1 (F 3, C & F). I GF - AM 711  
 FG1, FG1  
 FG1 (F 3, A-C),  
 m  
 (C m, 1997). B  
 2-1 FG, GF - AM 711 fi  
 FG1, FG1  
 m  
 (F 3, D-F).  
 2-1 FG FG1.

**The large vacuoles that form early block nuclear division at stage FG1**

FG  
 2-1 FG  
 A FG4, FG  
 (F 1K). B  
 2-1 FG  
 fi  
 FG (F 1L). A FG7, FG  
 (F 1M),  
 52.6% (=306) 2-1 FG  
 (F 1, & ),  
 m FG FG1 (43.6%  
 9% (& )) (F 1).

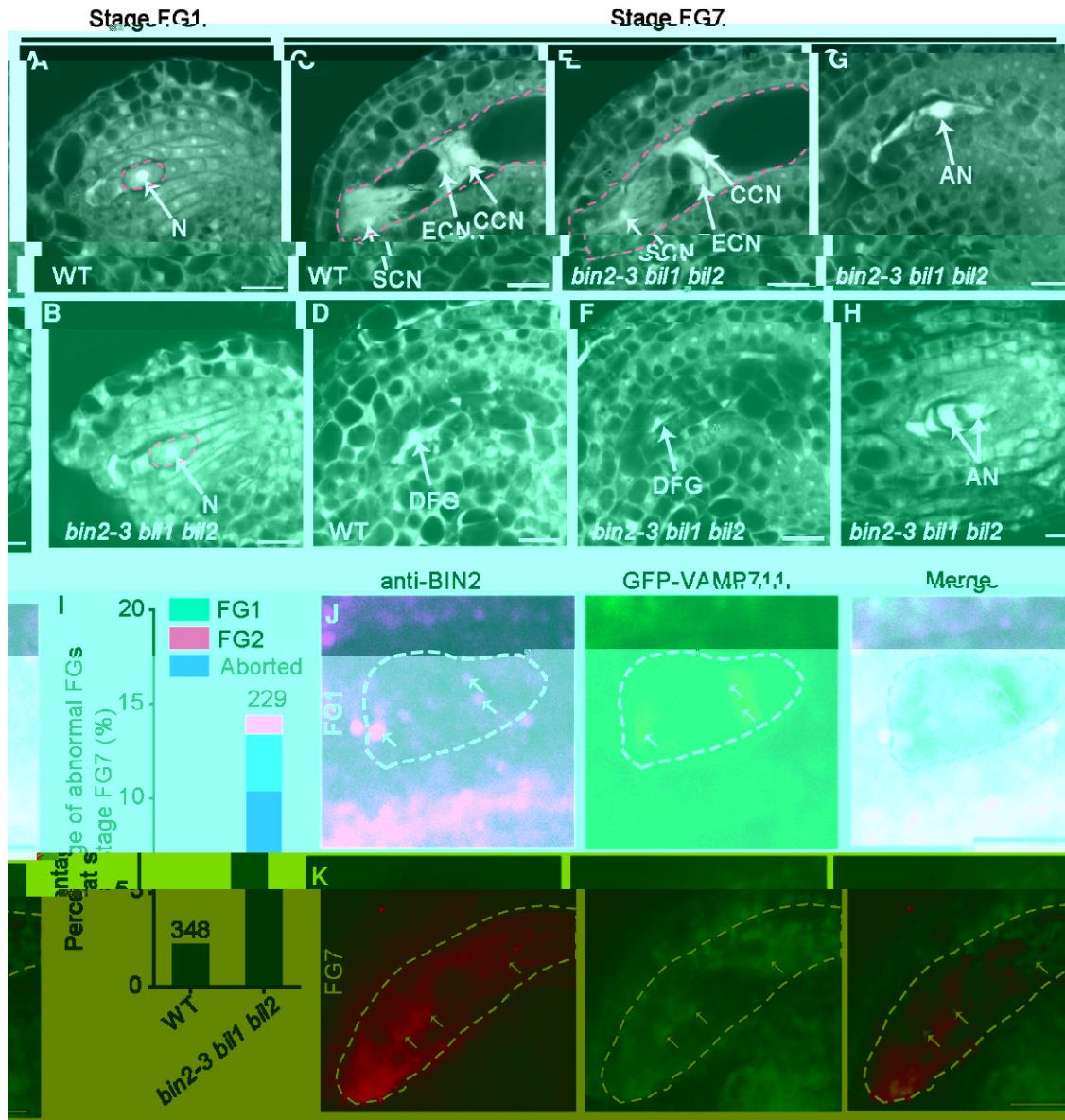


Figure 2 | *Bin2-3* mutant affects FG maturation. (A-I) Fluorescence microscopy images of FG1 and FG7 in WT and *bin2-3 bil1 bil2* mutant. (A) WT FG1. (B) *bin2-3 bil1 bil2* FG1. (C) WT FG7. (D) *bin2-3 bil1 bil2* FG7. (E-H) Immunofluorescence images of *bin2-3 bil1 bil2* mutant showing FG1 (E), FG2 (F), FG3 (G), and FG4 (H). (I) Bar graph showing the percentage of abnormal FGs at stage FG7. (J-K) Immunofluorescence images showing colocalization of anti-BIN2 (J) and GFP-VAMP711 (K) in WT and *bin2-3 bil1 bil2* mutant. Scale bars = 10 μm.

Figure 2 | *Bin2-3* mutant affects FG maturation. (A-I) Fluorescence microscopy images of FG1 and FG7 in WT and *bin2-3 bil1 bil2* mutant. (A) WT FG1. (B) *bin2-3 bil1 bil2* FG1. (C) WT FG7. (D) *bin2-3 bil1 bil2* FG7. (E-H) Immunofluorescence images of *bin2-3 bil1 bil2* mutant showing FG1 (E), FG2 (F), FG3 (G), and FG4 (H). (I) Bar graph showing the percentage of abnormal FGs at stage FG7. (J-K) Immunofluorescence images showing colocalization of anti-BIN2 (J) and GFP-VAMP711 (K) in WT and *bin2-3 bil1 bil2* mutant. Scale bars = 10 μm.

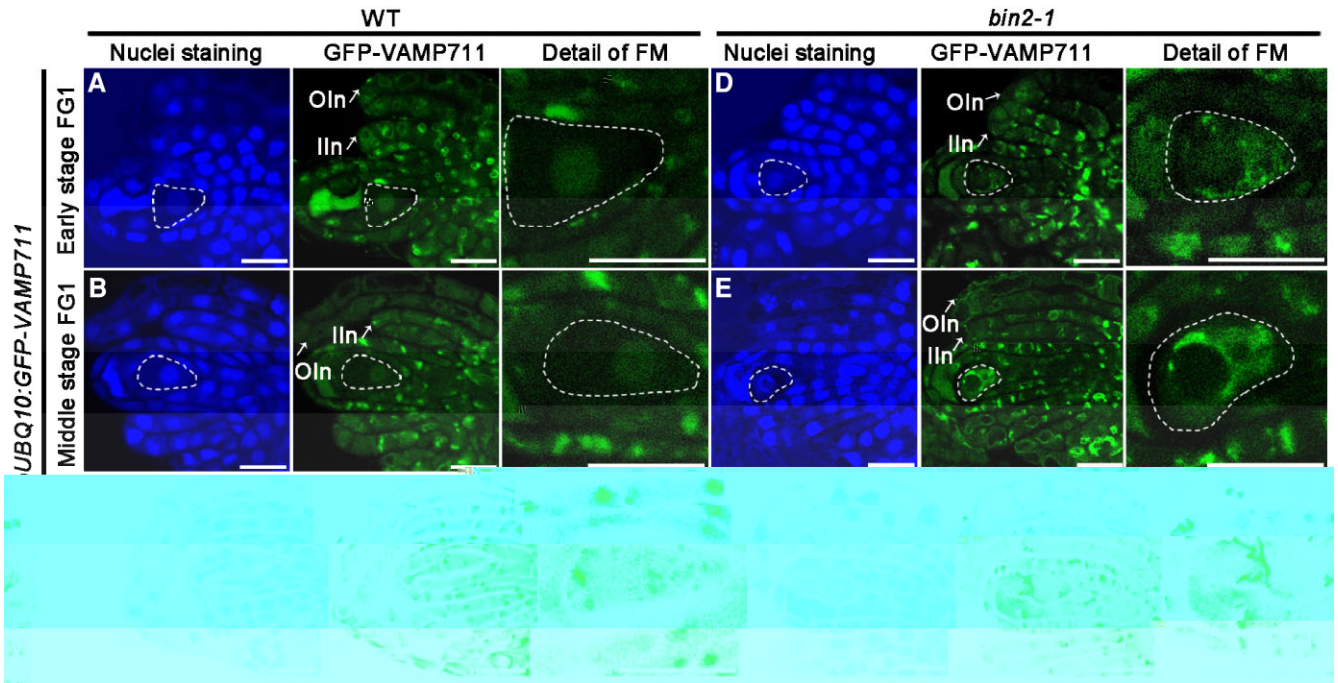


Figure 3. *bin2-1* affects the formation of female gametophyte (FG) vacuole. *bin2-1* mutant (A-F) and wild-type (WT) (A-C) female gametophyte (FG) cells were stained with DAPI (blue), GFP-VAMP711 (green), and FM (magenta) (A-F). Scale bars: (A-C) 10 μm, (D-F) 5 μm. *bin2-1* mutant (A-F) and wild-type (WT) (A-C) female gametophyte (FG) cells were stained with DAPI (blue), GFP-VAMP711 (green), and FM (magenta) (A-F). Scale bars: (A-C) 10 μm, (D-F) 5 μm. *bin2-1* mutant (A-F) and wild-type (WT) (A-C) female gametophyte (FG) cells were stained with DAPI (blue), GFP-VAMP711 (green), and FM (magenta) (A-F). Scale bars: (A-C) 10 μm, (D-F) 5 μm.

FG1 (Figure 1). *bin2-1* mutant (A-F) and wild-type (WT) (A-C) female gametophyte (FG) cells were stained with DAPI (blue), GFP-VAMP711 (green), and FM (magenta) (A-F). Scale bars: (A-C) 10 μm, (D-F) 5 μm. *bin2-1* mutant (A-F) and wild-type (WT) (A-C) female gametophyte (FG) cells were stained with DAPI (blue), GFP-VAMP711 (green), and FM (magenta) (A-F). Scale bars: (A-C) 10 μm, (D-F) 5 μm.

**BIN2 participates in female gametophyte development mainly by regulating vacuole formation**

*bin2-1* mutant (A-F) and wild-type (WT) (A-C) female gametophyte (FG) cells were stained with DAPI (blue), GFP-VAMP711 (green), and FM (magenta) (A-F). Scale bars: (A-C) 10 μm, (D-F) 5 μm. *bin2-1* mutant (A-F) and wild-type (WT) (A-C) female gametophyte (FG) cells were stained with DAPI (blue), GFP-VAMP711 (green), and FM (magenta) (A-F). Scale bars: (A-C) 10 μm, (D-F) 5 μm.

**BIN2 interacts with VLG both in vitro and in vivo**

*bin2-1* mutant (A-F) and wild-type (WT) (A-C) female gametophyte (FG) cells were stained with DAPI (blue), GFP-VAMP711 (green), and FM (magenta) (A-F). Scale bars: (A-C) 10 μm, (D-F) 5 μm. *bin2-1* mutant (A-F) and wild-type (WT) (A-C) female gametophyte (FG) cells were stained with DAPI (blue), GFP-VAMP711 (green), and FM (magenta) (A-F). Scale bars: (A-C) 10 μm, (D-F) 5 μm.

*bin2-1* mutant (A-F) and wild-type (WT) (A-C) female gametophyte (FG) cells were stained with DAPI (blue), GFP-VAMP711 (green), and FM (magenta) (A-F). Scale bars: (A-C) 10 μm, (D-F) 5 μm. *bin2-1* mutant (A-F) and wild-type (WT) (A-C) female gametophyte (FG) cells were stained with DAPI (blue), GFP-VAMP711 (green), and FM (magenta) (A-F). Scale bars: (A-C) 10 μm, (D-F) 5 μm.

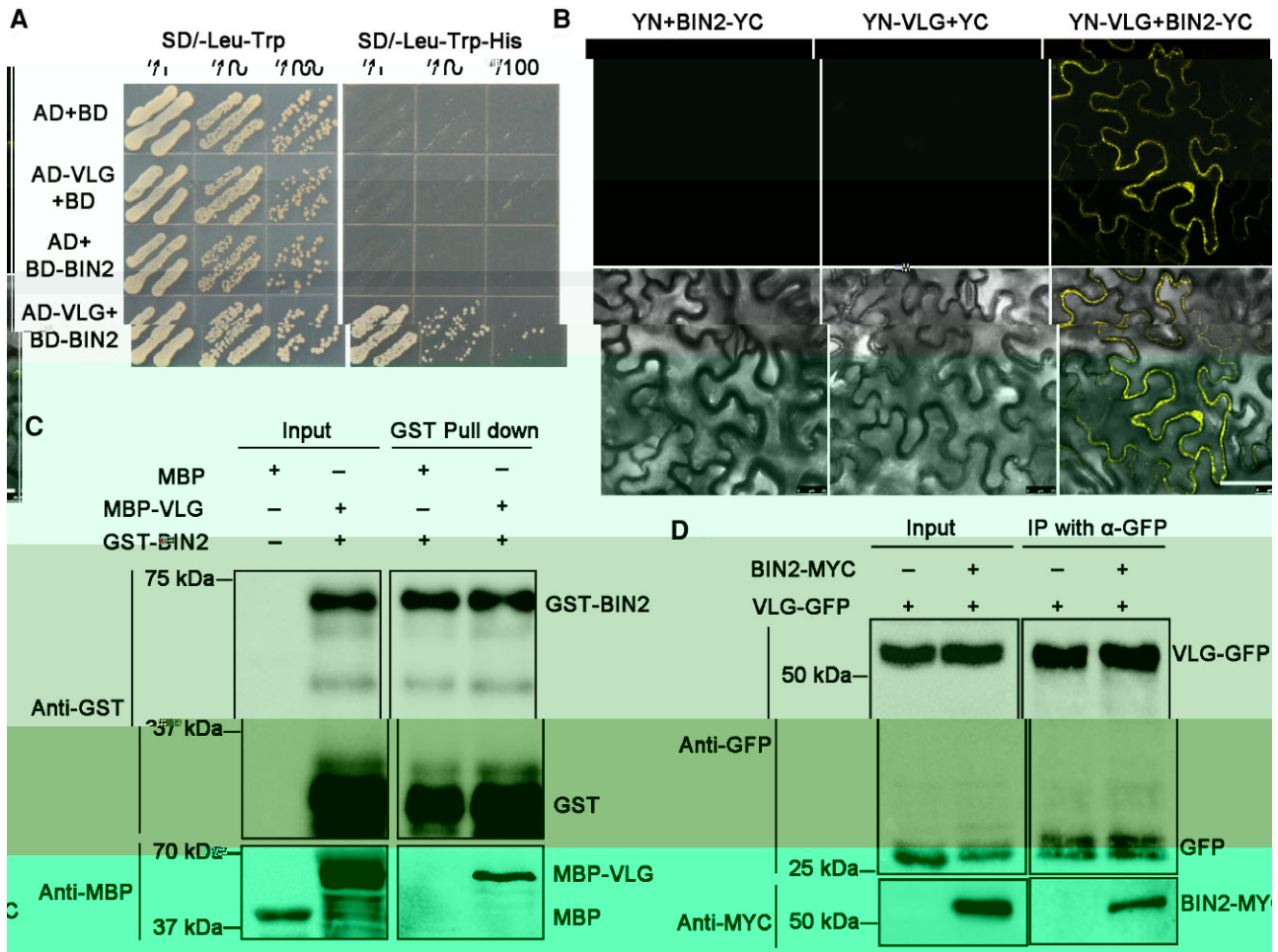


Figure 4. BIN2 positively regulates VLG abundance and influences large vacuole formation. (A) Yeast spot assay showing growth of various yeast strains on SD/-Leu-Trp and SD/-Leu-Trp-His media. (B) Fluorescence microscopy images of yeast cells expressing YN+BIN2-YC, YN-VLG+YC, and YN-VLG+BIN2-YC. (C) Co-immunoprecipitation assay showing interaction between MBP-VLG and GST-BIN2. (D) Co-immunoprecipitation assay showing interaction between BIN2-MYC and VLG-GFP.

... (Figs. 2-3, 5, A, B), ... BIN2 ...  
 ... FG (Figs. 2J-K, ... 2, 3; ... 2017), ...  
 ... BIN2 ... LG ...  
 ... FG ...

**BIN2 positively regulates VLG abundance and influences large vacuole formation**

BIN2 ... (K ... 2015). ... BIN2 ... LG ...  
 ... P, 35S: ...  
 ... VLG-GFP ... 2-1 ... 2-3 ... 1 ... 2 ... C ...  
 ... LG-GF ... fi ... 2-1 ...  
 ...

... 2-3 ... 1 ... 2 (Figs. 5, A, B), ... BIN2 ...  
 ... LG ...  
 ... LG ...  
 ... 2-1 FG ...  
 ... FG1, ... A ... (A) ...  
 ... FM1 ... fi ... VLG ...  
 ... (K ... 2004; H ... 2005).  
 ... P, FM1:VLG-RNA ... 2-1 (#1 ...  
 ... #2) ... fi ... LG ...  
 ... (Figs. 9A), ... FG ...  
 ... FG1 ... fi ...  
 ... (Figs. 5C). ... fi ...  
 ... VLG ...  
 ... FG1, ... fi ...  
 ... P, FM1:VLG-GFP ...  
 ... LG-GF ...  
 ... FG1 (Figs. 5D; ...  
 ... 9B). Im ...  
 ... FG7 ... fi ...



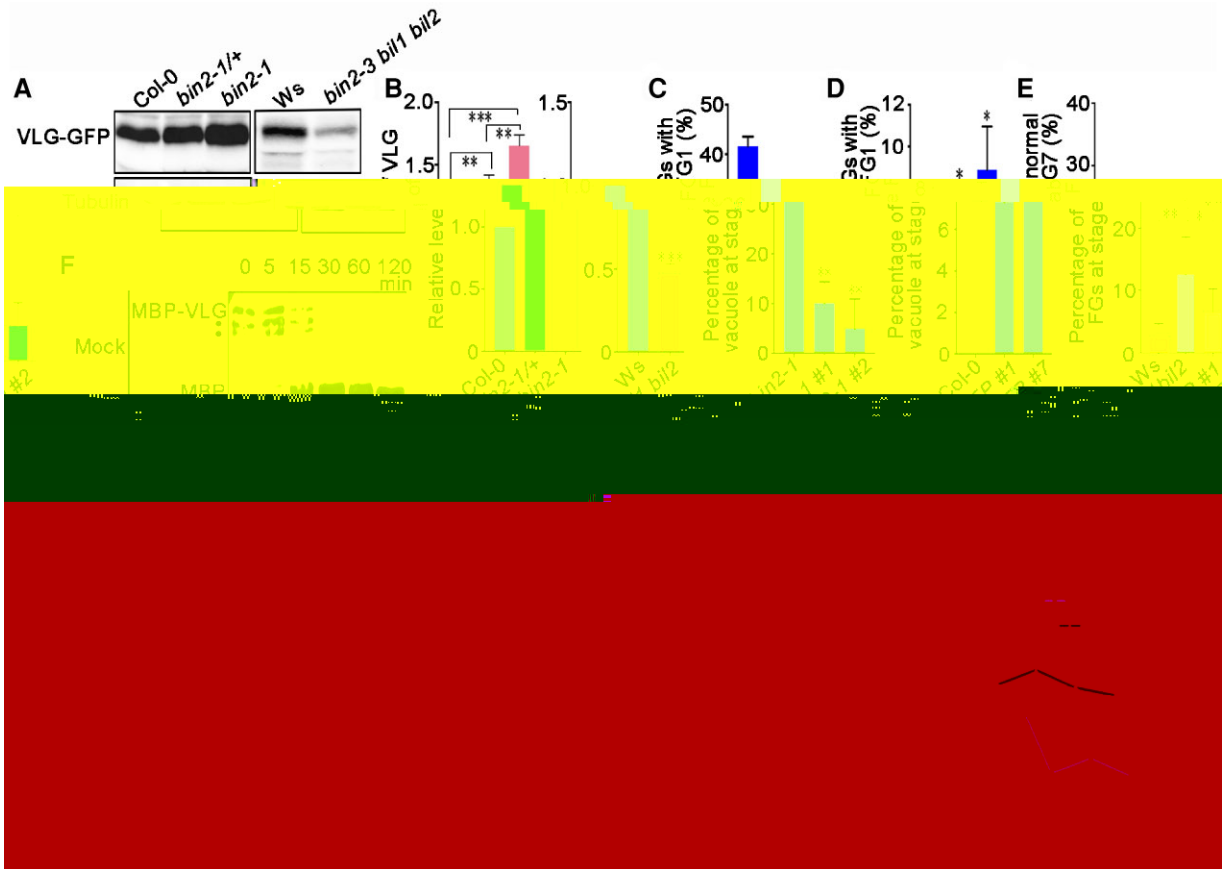


**Figure 5** BIN2-VLG modulates FG vacuole formation. (A–B) Western blot analysis and bar graph showing VLG-GFP levels and relative levels in Col-0, bin2-1/+, bin2-1, and Ws bin2-3 bil1 bil2. (C–E) Bar graphs showing the percentage of cells with G1 vacuoles, G1 vacuoles at stage, and normal G1 vacuoles. (F) Time course of MBP-VLG and Mock. (G–I) Bar graphs showing the percentage of FG1, FG2, and FG3 at stage. Error bars represent standard deviation. Statistical significance: \* $P < 0.05$ , \*\* $P < 0.01$ , \*\*\* $P < 0.001$ .

**BIN2 enhances VLG stability via phosphorylation**

Western blot analysis of VLG-GFP levels in Col-0, bin2-1/+, bin2-1, and Ws bin2-3 bil1 bil2. Tubulin is used as a loading control. (F 5E), (F 5F), (F 5G), (F 5H), (F 5I).

BI 2 LG  
 m. a. a. 26 LG. m.  
 B BI 2 LG, m  
 / / / / G K3  
 m (V A B), m LG  
 (F 6, A B), m LG  
 BI 2  
 m MB - LG MB -BI 2  
 LG m BI 2 (F 6C).  
 m (LC-M)  
 m LG MB - LG  
 MB -BI 2 BI 2  
 99, 103, 115, 119, 204, 208  
 G K3 LG  
 ( m / F 10). m  
 LG BI 2, m  
 m 99, 103, 115, 119, 204, 208  
 A  
 ( LG / -A) A  
 LG ( LG / -D).  
 LG / -A m  
 BI 2 LG  
 (F 6C). BI 2  
 LG m  
 BI 2 LG  
 (Cl) mm LG K3β LG  
 LG  
 Cl  
 G K3β (F 6D), BI 2 m LG  
 LG / -A m  
 LG / -A m  
 LG / -D m  
 (F 6E), LG / -A  
 LG / -D  
 BI 2-m  
 LG

**BIN2 might participate in large vacuole formation and female gametophyte development by phosphorylating VLG**

BI 2 fl LG FG  
 m P, FM1:  
 VLG<sup>S/T-A</sup>-GFP P, FM1:VLG<sup>S/T-D</sup>-GFP  
 m FG FG1 1  
 m P, FM1:VLG<sup>S/T-D</sup>-GFP  
 m 10% (#24) 4.1% (#30) FG  
 4.8% (#24) 3.3% (#30)  
 m 2-1 (F 7, A-E). P, FM1:  
 VLG<sup>S/T-A</sup>-GFP  
 8.1% (#7) 6.8% (#11) FG  
 ( m / F 11, A- 1D),

m 2-3 1 2, a, /VLG  
 (D' 1, 2017). I BI 2  
 m FG m  
 LG.  
 m LG  
 FG (F 8A). I BI 2  
 2-1 LG  
 26 m, m  
 FG1 (F 8B). B  
 BIN2 m 2-3 1  
 2 m LG m  
 m (F 8C).  
 B FG (F 8, B C).  
 C m  
 BI 2- LG  
 FG m

**Discussion**

FG  
 FG2 (C 1, 1997).  
 FG m ( 1, 2002; 1, 2015; D' 1, 2017). LG  
 /VLG m  
 FG1, FG2, FG7 (D' 1, 2017).  
 /VLG m ( ) m  
 FG2. H m  
 FG1  
 m  
 BI 2 G K3-  
 m ( / ) ( 1, 2002; 1, 2007, 2010),  
 m ( 1, 2019; L 1, 2020; 1, 2021; 1, 2021). I  
 BI 2  
 FG fl FG m BI 2  
 FG1  
 (F 1, C, F, I ),  
 BI 2 (F 1). L BIN2  
 2-3 1 2 m  
 FG (F 2H), BIN2 m  
 FG. m BI 2  
 fl LG, LG (F 6, C  
 E), fl m  
 m FG m BI 2 LG  
 FG,  
 LG m LG m  
 FG.

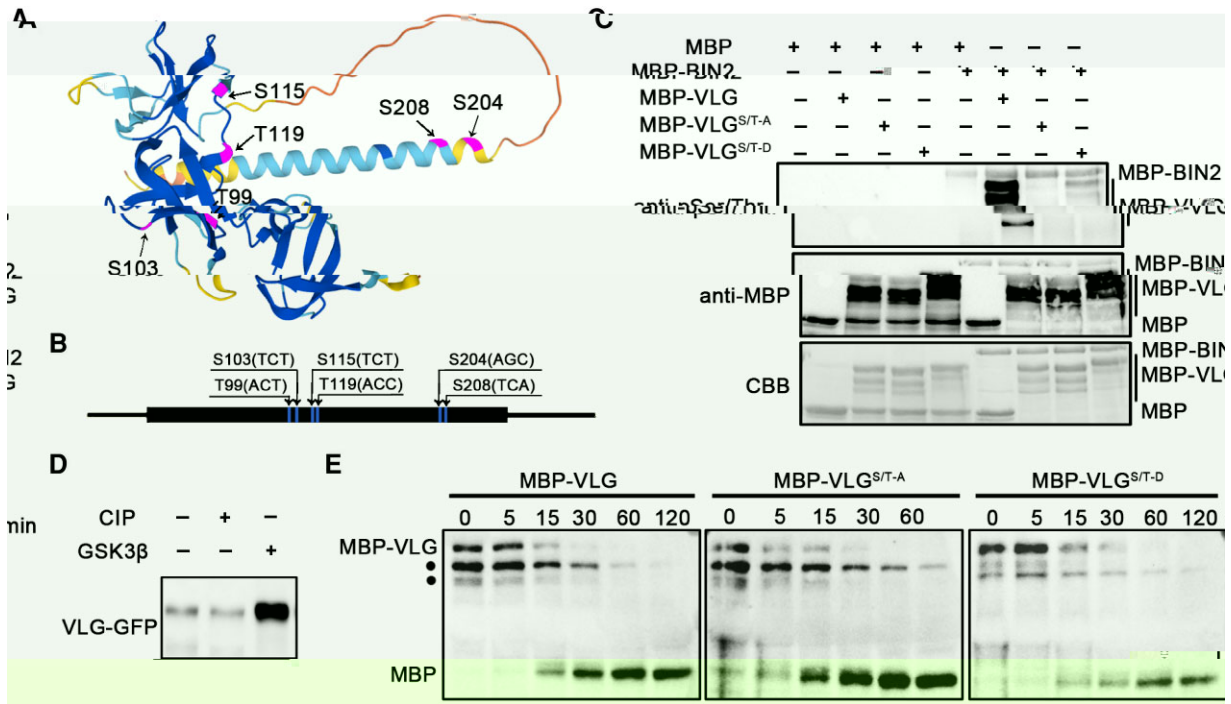
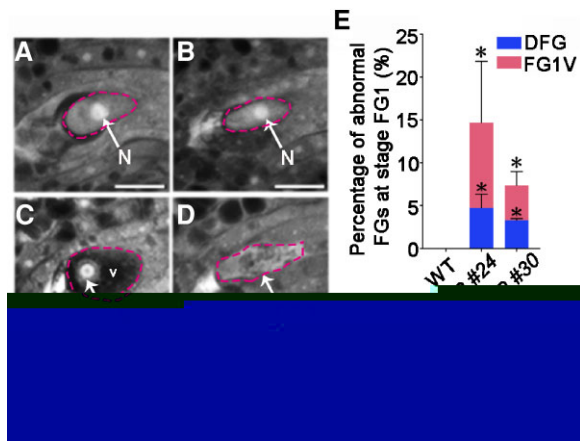


Figure 6. BIN2-VLG modulates FG vacuole formation. (A) 3D ribbon diagram of the BIN2 protein structure. Residues S103, T99, S115, T119, S208, and S204 are highlighted. (B) Schematic of the BIN2 protein with mutation sites S103(TCT)/T99(ACT), S115(TCT)/T119(ACC), and S204(AGC)/S208(TCA). (C) Western blot analysis showing co-immunoprecipitation of BIN2 with VLG variants. (D) Western blot analysis showing VLG-GFP. (E) Time-course Western blot analysis showing MBP-VLG variants (MBP-VLG, MBP-VLG<sup>S/T-A</sup>, MBP-VLG<sup>S/T-D</sup>) treated with CIP and GSK3β.



**Figure 7** (A) Root tip showing normal FG1 (white arrow). (B) Root tip showing abnormal FG1 (red dashed circle). (C) Root tip showing normal FG1 (white arrow). (D) Root tip showing abnormal FG1 (red dashed circle). (E) Bar graph showing the percentage of abnormal FG1s at stage FG1 for WT, #24, and #30 genotypes, comparing DFG (blue) and FG1V (red). Error bars represent standard deviation. \*P < 0.05.

(1 m / F 6),  
 2-1 (1 m / F 7),  
 FG  
 FG;  
 A  
 (1, 2021),  
 FG  
 BI 2- LG  
 FG  
 BI 2- LG

## Materials and methods

### Plant materials and growth conditions

(Cl B, 1998; 1999).  
 C-0, C-2, L M  
 C-0, 2-1 (L 2001),  
 P DD45:GFP (1999), P FM1:GUS (H  
 1999; 2005; 2020), P STK:BIN2\*-GFP (1999),  
 P 35S:BIN2-M C (1999).  
 2-3 1 2 1 m (1999)  
 C-2 P KNU:KNU-VENUS L  
 (1999; 2018). All A  
 22  
 C (16 / 8 ) fi  
 90 μm m<sup>-2</sup> (F L LED 8-16-65/  
 A22B/24 ).

### DNA manipulation

P UBQ10:GFP-VAMP711  
 G (1999). E  
 E /D/ (1999)  
 L- (L)  
 P UBQ10:GFP-GW  
 P UBQ10:GFP-VAMP711. A  
 C K (1999).  
 P 35S:VGL-GFP 747-  
 VLG (CD ) m fi  
 CAMBIA1302 (1999)  
 (2022) B II S I BIN2

(L [, 2002](#)), [, 2019](#))  
 P, BIN2:BIN2-GFP  
 P, UBQ10:GW-mC, P, VLG:GW-GFP,  
 P, FM1:GW-GFP, C M 35 HB  
 UBQ10, VLG, FM1  
 BIN2 VLG  
 P, UBQ10:BIN2-mC, P, FM1:VLG-GFP, P, VLG:  
 VLG-GFP, P, FM1:VLG-RNA  
 FM1 481- VLG-  
 FGCS941  
 (H [, 2005](#))  
 N, l. VLG- D A  
 K ( m), B mHI  
 LG CD (295  
 AC ACAA G C 309, 343 C G GCC GAGACC 357,  
 610 AGC CCGCGAA CA 624)  
 (295 GA ACAA G GA 309, 343 GA G GCC  
 GAGGAC 357, 610 GAC CCGCGAA GA 624)  
 (D),  
 P, FM1:VLG<sup>S/T-D</sup>-GFP (295  
 GC ACAA G GC 309, 343 GC G GCC GAGGCC  
 357, 610 GCC CCGCGAA GCA 624)  
 (A),  
 P, FM1:VLG<sup>S/T-A</sup>-GFP

HB  
 F B FC P, X104:  
 GW- FP P, X106; FP-GW  
 P, X104:BIN2- FP P, X106:  
 FP-VLG. F 2H  
 GBKT7 GADT7 [, 2019](#))  
 GBKT7-BIN2

M. M. ( B ) a m. E. 3  
m C A .ACTIN7 (A 5G09810)  
m m ( , 2019; J , 2020). All  
m m m m m m m  
m m m m m m m  
m m m m m m m  
m m m m m m m

### Confocal laser scanning microscopy

m m m m m m m  
m m m m m m m  
(C , 1997; , 2005). D  
m fix a m 30 m 4%  
a 12.5 m ( H 6.9).  
m fix m m  
m m m m m m m  
10%, 20%, 40%, 60%, 80%, 90% (10 m ). A  
90% b  
m m m m m m m  
m m m m m m m  
2:1 ( / )

100 C, 10 m. A 15- $\mu$ L (A m; AB0029; 1:3000), (A m; AB17464; 1:4,000).  
 1 m M A ) ( , 2019).  
 100 C, 10 m. A 15- $\mu$ L (A m; AB0029; 1:3000), (A m; AB17464; 1:4,000).

100 C, 10 m. A 15- $\mu$ L (A m; AB0029; 1:3000), (A m; AB17464; 1:4,000).

**Cell-free degradation assay**

F. 0.1 7- $\mu$ L (A m; AB0005; 1:3000).  
 (25 m M -HCl, H 7.5, 10 m M Cl<sub>2</sub>, 10 m M Cl<sub>2</sub>, 5 m M D , 0.4 m M F, 10 m M A ) 30 m . 1  $\mu$  M B - LG 22 C 100 C, 10 m . D - AGE. (A m; AB0029; 1:3000).

**Immunoblot assay**

F. 7- $\mu$ L (A m; AB0005; 1:5,000).  
 2X D 18,514 10 m 4 C. 10 m . 10  $\mu$ L 10% D - AGE (A m; A 163203; 1:5,000).  
 F 2B, -GF (A m; AB0005; 1:5,000).  
 (A m; 20045; 1:5,000). F 5, A H 4 C.  
 G -m G (H+L) H ( B.; B-AB0102; 1:5,000). G (H+L) H ( B.; B-AB0101; 1:5,000). All 5% m ( B 1% -20).  
 B1 - AD C m D. Im LG F 5, A H Im L (B. - a) ( , 2019).

**CIP and GSK treatment assays**

F. Cl m , LG-GF mm GF - B1 a Cl ( m ) 2  $\mu$ L Cl ( E / a B ) . 500  $\mu$ L Cl (50 m M -HCl, H 7.5, 5 m M Cl<sub>2</sub>, 1 m M D , 1 m M F, 0.1% -40) 60 m 37 C. LG-GF mm GF - 2  $\mu$ L G K3 $\beta$  300  $\mu$ L G K3 $\beta$  60 m 37 C mm B1 . 100 C, 10 m . A 20- $\mu$ L -GF (A m; AB0005; 1:3000).

**Root mitosis analysis**

1/2X m m 7–10 fix C fix (100% =3:1) ( , 2014).  
 m m fix m H<sub>2</sub> 20 m 37 C. A H<sub>2</sub> 45 C, 30 , 20  $\mu$ L, 60% 20- $\mu$ L (-20 C) C fix 5–10 m . A 7–10  $\mu$ L DA I, A A2 m ( , 2014).

**kinase treatment assay**

M B - LG M B - B1 2 m m 5  $\mu$  M B M B - B1 2 20  $\mu$  m B M B - LG 30 C, 1 (25 m M -HCl H 7.4, 12 m M Cl<sub>2</sub>, 1 m M D

**Accession numbers**

ACTIN7 (A 5G09810), AGP18 (A 4G37450), AGL23 (A 1G65360), AOG1 (A 5G57790), ATKIN-1 (A 3G63480), BIN2 (A 4G18710), BIL1 (A 2G30980), BIL2 (A 1G06390), BUB3.1 (A 3G19590), C CA1;1 (A 1G44110), C CB2;3

(A 1G20610), C CD2;1 (A 2G22490), C CD3;1 (A 4G34160), DD45 (A 2G21740), D AD (A 5G51330), FM1 (A 4G12250), KNU (A 5G14010), MOS7 (A 5G05680), PRL (A 4G02060), SNAIL1 (A 5G61770), SWA1 (A 2G47990), SWA2 (A 1G72440), VLG (A 2G17740).

## Supplemental data

- [Supplemental Figure S1.](#)
- [Supplemental Figure S2.](#)
- [Supplemental Figure S3.](#)
- [Supplemental Figure S4.](#)
- [Supplemental Figure S5.](#)
- [Supplemental Figure S6.](#)
- [Supplemental Figure S7.](#)
- [Supplemental Figure S8.](#)
- [Supplemental Figure S9.](#)
- [Supplemental Figure S10.](#)
- [Supplemental Figure S11.](#)
- [Supplemental Figure S12.](#)
- [Supplemental Data Set S1.](#)
- [Supplemental Data Set S2.](#)

## Acknowledgments



- C // H 174(3): 1609–1620
- Gomez MD, Barro-Trastoy D, Fuster-Almunia C, Tornero P, Alonso JM, Perez-Amador MA (2020) G // GA-LIKE1 A // J E. B. 71(22): 7059–7072
- Hu ZB, Qin ZX, Wang M, Xu CY, Feng GP, Liu J, Meng Z, Hu YX (2010) A // 2, m. 112, m. 600–610
- Huanca-Mamani W, Garcia-Aguilar M, León-Martínez G, Grossniklaus U, Vielle-Calzada JP (2005) CH 11, A // A 102(47): 17231–6
- Jiang HL, Hong J, Jiang YT, Yu SX, Zhang YJ, Shi JX, Lin WH (2020) G // A // (B ) 9(5): 585
- Jonak C, Hirt H (2002) G // 3/ HAGG // 7(10): 457–461
- Kerschen A, Napoli CA, Jorgensen RA, Müller AE (2004) E // FEB L 566(1–3): 223–228
- Kim TW, Guan S, Sun Y, Deng Z, Tang W, Shang JX, Sun Y, Burlingame AL, Wang ZY (2009) B // C // B. // 11(10): 1254–1260
- Klein PS, Melton DA (1996) A // A 93(16): 8455–8459
- Kooiker M, Airoidi CA, Losa A, Manzotti PS, Finzi L, Kater MM, Colombo L (2005) BA IC E AC EI E1, GA // EED ICK. // C // 17(3): 722–729
- Kurihara D, Mizuta Y, Sato Y, Higashiyama T (2015) C // D // 142(23): 4168–4179
- Latrasse D, Benhamed M, Henry Y, Domenichini S, Kim W, Zhou DX, Delarue M (2008) // B/C // B. // 8(1): 121
- Laube U, Kiderlen AF (1998) D // H33258 // 84(7): 559–564
- Lermontova I, Fuchs J, Schubert I (2008) A // B 3.1 // 13(13): 5202–5211
- Li J, Nam KH, Vafeados D, Chory J (2001) BI 2, A // 127(1): 14–22
- Li J, Terzaghi W, Gong Y, Li C, Ling JJ, Fan Y, Qin N, Gong X, Zhu D, Deng XW (2020) // BI 2 // H 5 // C. mm // 11(1): 1592
- Li JM, Nam KH (2002) // G K3/ HAGG // 295(5558): 1299–1301
- Liu F, Li JP, Li LS, Liu Q, Li SW, Song ML, Li S, Zhang Y (2021) // A // L G // 17(4): 1009505
- Liu J, Zhang Y, Qin G, Tsuge T, Sakaguchi N, Luo G, Sun K, Shi D, Aki S, Zheng N, et al. (2008) // ICK4/K 6. I G- E3 // C // 20(6): 1538–1554
- Maiti S, Maiti P, Sinha SS, Mitra RK, Pal SK (2009) // D A: // I J B. // 44(2): 133–137
- Matias-Hernandez L, Battaglia R, Galbiati F, Rubes M, Eichenberger C, Grossniklaus U, Kater MM, Colombo L (2010) E DA DII // MAD // A // C // 22(6): 1702–1715
- Menges M, Samland AK, Planchais S, Murray JAH (2006) D- // C CD3;1 // G1- // A // C // 18(4): 893–906
- Modrusan Z, Reiser L, Feldmann KA, Fischer RL, Haughn GW (1994) H. m. // A // C // 6(3): 333–349
- Murashige T, Skoog F (1962) A // 15(3): 473–497
- Panoli A, Martin MV, Alandete-Saez M, Simon M, Neff C, Swarup R, Bellido A, Yuan L, Pagnussat GC, Sundaresan V (2015) A // L // 10(5): 0126164
- Park GT, Frost JM, Park JS, Kim TH, Lee JS, Oh SA, Twell D, Brooks JS, Fischer RL, Choi Y (2014) // 7/ 88 // A // A 111(51): 18393–8
- Payne T, Johnson SD, Koltunow AM (2004) K CKLE (K ) // C2H2 // A // 131- (15): 3737–3749
- Pinyopich A, Ditta GS, Savidge B, Liljegren SJ, Baumann E, Wisman E, Yanofsky MF (2003) A // MAD

- Vert G, Chory J (2006) *D* 441(7089): 96–100
- Wang H, Liu R, Wang J, Wang P, Shen Y, Liu G (2014) *A* 33(5): 819–828
- Wang J, Guo X, Xiao Q, Zhu J, Cheung AY, Yuan L, Vierling E, Xu S (2021) *A* 230(6): 2261–2274
- Wang Y, Cheng Z, Lu P, Timofejeva L, Ma H (2014) *A* 1110: 217–230
- Wang Z, Meng P, Zhang X, Ren D, Yang S (2011) *B* 67(6): 1081–1093
- Wang ZY, Nakano T, Gendron J, He J, Chen M, Vafeados D, Yang Y, Fujioka S, Yoshida S, Asami T, et al. (2002) *D* 2(4): 505–513
- Webb MC, Gunning BES (1990) *Em* 3(4): 244–256
- West M, Harada JJ (1993) *Em* 5(10): 1361–1369
- Wu JJ, Peng XB, Li WW, He R, Xin HP, Sun MX (2012) *M* 23(5): 1043–1058
- Xiong F, Duan CY, Liu HH, Wu JH, Zhang ZH, Li S, Zhang Y (2020) *A* KETCH1
- Xu P, Lian H, Xu F, Zhang T, Wang S, Wang W, Du S, Huang J, Yang HQ (2019) *B* AGB1
- A* 12(2): 229–247
- Yan Z, Zhao J, Peng P, Chihara RK, Li J (2009) *BI 2 F* 150(2): 710–721
- Ye K, Li H, Ding Y, Shi Y, Song C, Gong Z, Yang S (2019) *B A I E* ID-I E I I E2 ICE1
- A* 31(11): 2682–2696
- Youn JH, Kim TW (2015) *F* G K3-L 8(4): 552–565
- Yu SX, Zhou LW, Hu LQ, Jiang YT, Zhang YJ, Feng SL, Jiao Y, Xu L, Lin WH (2020) *A* 147(24): 196618
- Zhang DW, Tan WR, Yang F, Han Q, Deng XG, Guo HQ, Liu BH, Yin YH, Lin HH (2021) *A BI 2-GLK1* D C 56(3): 310–324. 7
- Zhang YJ, Zhang Y, Zhang LL, He JX, Xue HW, Wang JW, Lin WH (2022) *GA A6* 73(18): 6133–6149
- Zhao L, Cai H, Su Z, Wang L, Huang X, Zhang M, Chen P, Dai X, Zhao H, Palanivelu R, et al. (2018) *KLU* 1-m WRK 28 A 115(3): E526–EE35
- Zu SH, Jiang YT, Hu LQ, Zhang YJ, Chang JH, Xue HW, Lin WH (2019) *E* 10: 980